Structural analysis of SARS-CoV-2 and predictions of the human interactome

Andrea Vandelli[1,2], Michele Monti[1,3], Edoardo Milanetti[4,5],
Jakob Rupert [6], Elsa Zacco[3], Elias Bechara[1,3],
Riccardo Delli Ponti [7,*] and Gian Gaetano Tartaglia [1,3,6,8,*]

[1] Centre for Genomic Regulation (CRG), The Barcelona Institute for Science and Technology, Dr. Aiguader 88, 08003 Barcelona, Spain and Universitat Pompeu Fabra (UPF), 08003 Barcelona, Spain
[2] Systems Biology of Infection Lab, Department of Biochemistry and Molecular Biology, Biosciences Faculty, Universitat Autònoma de Barcelona, 08193 Cerdanyola del Vallès, Spain
[3] Department of Neuroscience and Brain Technologies, Istituto Italiano di Tecnologia, Via Morego 30, 16163, Genoa, Italy.
[4] Department of Physics, Sapienza University, Piazzale Aldo Moro 5, 00185, Rome, Italy
[5] Center for Life Nanoscience, Istituto Italiano di Tecnologia, Viale Regina Elena 291, 00161, Rome, Italy
[6] Department of Biology 'Charles Darwin', Sapienza University of Rome, P.le A. Moro 5, Rome 00185, Italy
[7] School of Biological Sciences, Nanyang Technological University, 60 Nanyang Drive, Singapore, 637551, Singapore
[8] Institucio Catalana de Recerca i Estudis Avançats (ICREA), 23 Passeig Lluis Companys, 08010 Barcelona, Spain

*to whom correspondence should be addressed to: riccardo.ponti@ntu.edu.sg (RDP) and giangaetano.tartaglia@uniroma1.it or gian.tartaglia@iit.it (GGT)

ABSTRACT

Specific elements of viral genomes regulate interactions within host cells. Here, we calculated the secondary structure content of >2500 coronaviruses and computed >100000 human protein interactions with severe acute respiratory syndrome coronavirus 2 (SARS-CoV-2). We found that the 3' and 5' are the most structured elements in the viral genome and the 5' has the strongest propensity to associate with human proteins. The domain encompassing nucleotides 23000 – 24000 is highly conserved both at the sequence and structural level, while the region upstream varies significantly. These two sequences code for a domain of the viral protein Spike S that interacts with the human receptor angiotensin-converting enzyme 2 (ACE2) and has the potential to bind sialic acids. Our predictions indicate that the first 1000 nucleotides in the 5' can interact with proteins

involved in viral RNA processing such as double-stranded RNA specific editases and ATP-dependent RNA-helicases, in addition to other high-confidence candidate partners. These interactions, previously reported to be also implicated in HIV, reveal important information on host-virus interactions. The list of transcriptional and post-transcriptional elements recruited by SARS-CoV-2 genome provides clues on the biological pathways associated with gene expression changes in human cells.

INTRODUCTION

A disease named Covid-19 by the World Health Organization and caused by the severe acute respiratory syndrome coronavirus 2 (SARS-CoV-2) has been recognized as responsible for the pneumonia outbreak that started in December, 2019 in Wuhan City, Hubei, China [1] and spread in February to Milan, Lombardy, Italy [2] becoming pandemic. As of April 2020, the virus infected >2'000'000 people in >200 countries.

SARS-CoV-2 is a positive-sense single-stranded RNA virus that shares similarities with other beta-coronavirus such as severe acute respiratory syndrome coronavirus (SARS-CoV) and Middle East respiratory syndrome coronavirus (MERS-CoV) [3]. Bats have been identified as the primary host for SARS-CoV and SARS-CoV-2 [4,5] but the intermediate host linking SARS-CoV-2 to humans is still unknown, although a recent report indicates that pangolins could be involved [6].

Coronaviruses use species-specific proteins to mediate the entry in the host cell and the spike S protein activates the infection in human respiratory epithelial cells in SARS-CoV, MERS-CoV and SARS-CoV-2 [7]. Spike S is assembled as a trimer and contains around 1,300 amino acids within each unit [8,9]. The receptor binding domain (RBD) of Spike S, which contains around 300 amino acids, mediates the binding with angiotensin-converting enzyme, (ACE2) attacking respiratory cells. Another region upstream of the RBD, present in MERS-CoV but not in SARS-CoV, is involved in the adhesion to sialic acid and could play a key role in regulating viral infection [7,10].

At present, very few molecular details are available on SARS-CoV-2 and its interactions with the human host, which are mediated by specific RNA elements [11]. To study the RNA structural content, we used *CROSS* [12] that was previously developed to investigate large transcripts such as the human immunodeficiency virus HIV-1 [13]. *CROSS* predicts the structural profile of RNA molecules (single-

and double-stranded state) at single-nucleotide resolution using sequence information only. Here, we performed sequence and structural alignments among 62 SARS-CoV-2 strains and identified the conservation of specific elements in the spike S region, which provides clues on the evolution of domains involved in the binding to ACE2 and sialic acid.

As highly structured regions of RNA molecules have strong propensity to form stable contacts with proteins [14] and promote assembly of specific complexes [15,16], SARS-CoV-2 domains enriched in double-stranded content are expected to establish interactions within host cells that are important to replicate the virus [17]. To investigate the interactions of SARS-CoV-2 RNA with human proteins, we employed *cat*RAPID [18,19]. *cat*RAPID [20] estimates the binding potential of a specific protein for an RNA molecule through van der Waals, hydrogen bonding and secondary structure propensities allowing identification of interaction partners with high confidence [21]. The unbiased analysis of more than 100000 protein interactions with SARS-CoV-2 RNA reveals that the 5' of SARS-CoV-2 has strong propensity to bind to human proteins involved in viral infection and especially reported to be associated with HIV infection. A comparison between SARS-CoV and HIV reveals indeed similarities [22], but the relationship between SARS-CoV-2 and HIV is still unexplored. Interestingly, HIV and SARS-CoV-2, but not SARS-CoV nor MERS-CoV, have a furin-cleavage site occurring in the spike S protein, which could explain the spread velocity of SARS-CoV-2 compared to SARS-CoV and MERS-CoV [23,24]. Yet, many processes related to SARS-CoV-2 replication are unknown and our study aims to suggest relevant protein interactions for further investigation.

We hope that our large-scale calculations of structural properties and binding partners of SARS-CoV-2 will be useful to identify the mechanisms of virus replication within the human host.

RESULTS

SARS-CoV-2 contains highly structured elements

Structured elements within RNA molecules attract proteins [14] and reveal regions important for interactions with the host [25]. Indeed, each gene expressed from SARS-CoV-2 is preceded by conserved transcription-regulating sequences that act as signal for the transcription complex during the synthesis of the RNA minus strand to promote a strand transfer to the leader region to resume the synthesis. This process is named discontinuous extension of the minus strand and is a variant of similarity-assisted template switching that operates during viral RNA recombination [17].

104

105 To analyze SARS-CoV-2 structure (reference Wuhan strain MN908947.3), we employed *CROSS* [12]
106 to predict the double- and single-stranded content of RNA genomes such as HIV-1 [13]. We found the
107 highest density of double-stranded regions in the 5' (nucleotides 1-253), membrane M protein
108 (nucleotides 26523-27191), spike S protein (nucleotides 23000-24000), and nucleocapsid N protein
109 (nucleotides 2874-29533; **Fig. 1**) [26]. The lowest density of double-stranded regions were observed
110 at nucleotides 6000-6250 and 20000-21500 and correspond to the regions between the non-
111 structural proteins nsp14 and nsp15 and the upstream region of the spike surface protein S (**Fig. 1**)
112 [26]. In addition to the maximum corresponding to nucleotides 23000-24000, the structural content of
113 spike S protein shows minima at around nucleotides 20500 and 24500 (**Fig. 1**).
114 We used the *Vienna* method [27] to further investigate the RNA secondary structure of specific
115 regions identified with *CROSS* [13]. Employing a 100 nucleotide window centered around *CROSS*
116 maxima and minima, we found good match between *CROSS* scores and Vienna free energies (**Fig.**
117 **1).** Strong agreement is also observed between *CROSS* and *Vienna* positional entropy, indicating
118 that regions with the highest structural content have also the lowest structural diversity.
119
120 Our analysis suggests the presence of structural elements in SARS-CoV-2 that have evolved to
121 interact with specific human proteins [11]. Our observation is based on the assumption that structured
122 regions have an intrinsic propensity to recruit proteins [14], which is supported by the fact that
123 structured transcripts act as scaffolds for protein assembly [15,16].
124
125
126 **Structural comparisons reveal that the spike S region of SARS-CoV-2 is conserved among**
127 **coronaviruses**
128
129 We employed *CROSS*align [13] to study the structural conservation of SARS-CoV-2 in different
130 strains (**Materials and Methods**).
131
132 In our analysis, we compared the Wuhan strain MN908947.3 with around 2800 other coronaviruses
133 (data from NCBI) with human (**Fig. 2**) or other hosts (**Supp. Fig. 1**). When comparing SARS-CoV-
134 2 with human coronaviruses (1387 strains, including SARS-CoV and MERS-CoV), we found that
135 the most conserved region falls inside the spike S genomic locus (**Fig. 2**). More precisely, the
136 conserved region is between nucleotides 23000 - 24000 and exhibits an intricate and stable

137 secondary structure (RNA*fold* minimum free energy= -269 kcal/mol)[27]. High conservation of a
138 structured region suggests a functional activity that might be relevant for host infection.
139
140 The 3' and 5' of SARS-CoV-2 are highly variable in our set. However, the 3' and 5' are more
141 structured in SARS-CoV-2 than other coronaviruses (average structural content for SARS-CoV-2 =
142 0.56, indicating that 56% of the CROSS signal is >0, in the 5' and 0.49 in the 3'; by contrast, other
143 coronaviruses have 0.49 in the 5' and 0.42 in the 3').
144
145
146 **Sequence and structural comparisons among SARS-CoV-2 strains indicate conservation of**
147 **the ACE2 binding site and high variability in a region potentially interacting with sialic acids.**
148
149 To better investigate the sequence conservation of SARS-CoV-2, we compared 62 strains isolated
150 from different countries during the pandemic (including China, USA, Japan, Taiwan, India, Brazil,
151 Sweden, and Australia; data from NCBI and in VIPR www.viprbrc.org; **Materials and Methods**).
152 Our analysis aims to determine the relationship between structural content and sequence
153 conservation.
154
155 Using *Clustal W* for multiple sequence alignments [28], we observed general conservation of the
156 coding regions (**Fig. 3A**). The 5' and 3' show high variability due to experimental procedures of the
157 sequencing and are discarded in this analysis [29] . One highly conserved region is between
158 nucleotides 23000 - 24000 in the spike S genomic locus, while sequences up- and downstream are
159 variable (red bars in **Fig. 3A**). We then used CROSS*align* [13] to compare the structural content
160 (**Materials and Methods**). High variability of structure is observed for both the 5' and 3' and for
161 nucleotides between 21000 - 22000 as well as 24000 - 25000, associated with the S region (red bars
162 in **Fig. 3A**). The rest of the regions are significantly conserved at a structural level (p-value <
163 0.0001; Fisher's test).
164
165 We then compared protein sequences coded by the spike S genomic locus (NCBI reference
166 QHD43416) and found that both sequence (**Fig. 3A**) and structure (**Fig. 2**) of nucleotides 23000 -
167 24000 are highly conserved. The region corresponds to amino acids 330-500 that contact the host
168 receptor angiotensin-converting enzyme 2 (ACE2) [30] promoting infection and provoking lung injury
169 [24,31]. By contrast, the region upstream of the binding site receptor ACE2 and located in
170 correspondence to the minimum of the structural profile at around nucleotides 22500-23000 (**Fig. 1**)

171 is highly variable [32], as indicated by *T-coffee* multiple sequence alignments [32] (**Fig. 3A**). This part of
172 the spike S region corresponds to amino acids 243-302 that in MERS-CoV binds to sialic acids
173 regulating infection through cell-cell membrane fusion (**Fig. 3B;** see related manuscript by E.
174 Milanetti *et al*.) [10,33,34].
175
176 Our analysis suggests that the structural region between nucleotides 23000 and 24000 of Spike S
177 region is conserved among coronaviruses (**Fig. 2**) and that the binding site for ACE2 has poor
178 variation in human SARS-CoV-2 strains (**Fig. 3B**). By contrast, the region upstream, which has
179 propensity to bind sialic acids [10,33,34], showed poor structural content and high variability (**Fig. 3B**).
180
181 **Analysis of human interactions with SARS-CoV-2 identifies proteins involved in viral**
182 **replication**
183
184 In order to obtain insights on how the virus replicates in human cells, we predicted SARS-CoV-2
185 interactions with the whole RNA-binding human proteome. Following a protocol to study structural
186 conservation in viruses [13], we first divided the Wuhan sequence in 30 fragments of 1000 nucleotides
187 each moving from the 5' to 3' and then calculated the protein-RNA interactions of each fragment
188 with *cat*RAPID *omics* (3340 canonical and putative RNA-binding proteins, or RBPs, for a total
189 102000 interactions) [18]. Proteins such as Polypyrimidine tract-binding protein 1 PTBP1 (Uniprot
190 P26599) showed the highest interaction propensity (or Z-score; **Materials and Methods**) at the 5'
191 while others such as Heterogeneous nuclear ribonucleoprotein Q HNRNPQ (O60506) showed the
192 highest interaction propensity at the 3', in agreement with previous studies on coronaviruses (**Fig.**
193 **4A**) [35].
194
195 For each fragment, we predicted the most significant interactions by filtering according to the Z
196 score. We used three different thresholds in ascending order of stringency: Z ≥ 1.50, 1.75 and 2
197 respectively and we removed from the list the proteins that were predicted to interact promiscuously
198 with more than one fragment. Fragment 1 corresponds to the 5' and is the most contacted by RBPs
199 (around 120 with Z≥2 high-confidence interactions; **Fig. 4B**), which is in agreement with the
200 observation that highly structured regions attract a large number of proteins [14]. Indeed, the 5'
201 contains multiple stem loop structures that control RNA replication and transcription [36,37]. By
202 contrast, the 3' and fragment 23 (Spike S), which are still structured but to a lesser extent, attract
203 fewer proteins (10 and 5, respectively), while fragment 20 (between orf1ab and Spike S) that is
204 predicted to be unstructured, does not have binding partners.

205

206 The interactome of each fragment was then analysed using *clever*GO, a tool for Gene Ontology
207 (GO) enrichment analysis [38]. Proteins interacting with fragments 1, 2 and 29 were associated with
208 annotations related to viral processes (**Fig. 4C; Supp. Table 1**). Considering the three thresholds
209 applied (**Materials and Methods**), we found 22 viral proteins for fragment 1, 2 proteins for
210 fragment 2 and 11 proteins for fragment 29 (**Fig. 4D**).

211

212 Among the high-confidence interactors of fragment 1, we discovered RBPs involved in positive
213 regulation of viral processes and viral genome replication, such as double-stranded RNA-specific
214 editase 1 ADARB1 (Uniprot P78563 [39]), 2-5-oligoadenylate synthase 2 OAS2 (P29728) and 2-5A-
215 dependent ribonuclease RNASEL (Q05823). Interestingly, 2-5-oligoadenylate synthase 2 OAS2 has
216 been reported to be upregulated in human alveolar adenocarcinoma (A549) cells infected with
217 SARS-CoV-2 (log fold change of 4.2; p-value of 10^{-9} and q-value of 10^{-6}) [40]. While double-stranded
218 RNA-specific adenosine deaminase ADAR (P55265) is absent in our library due to its length that
219 does not meet *cat*RAPID *omics* requirements [18], the *omiXcore* extension of the algorithm
220 specifically developed for large molecules [41] attributes the same binding propensity to both
221 ADARB1 and ADAR, thus indicating that the interactions might occur (**Materials and Methods**).
222 Moreover, experimental works indicate that the family of ADAR deaminases is active in
223 bronchoalveolar lavage fluids derived from SARS-CoV-2 patients [42] and is upregulated in A549
224 cells infected with SARS-CoV-2 (log fold change of 0.58; p-value of 10^{-8} and q-value of 10^{-5}) [40].

225

226 We also identified proteins related to the establishment of integrated proviral latency, including X-
227 ray repair cross-complementing protein 5 XRCC5 (P13010) and X-ray repair cross-complementing
228 protein 6 XRCC6 (P12956; **Fig. 4B** and **4E**). In accordance with our calculations, comparison of
229 A549 cells responses to SARS-CoV-2 and respiratory syncytial virus, indicates upregulation of
230 XRRC6 in SARS-CoV-2 (log fold-change of 0.92; p-value of 0.006 and q-value of 0.23) [40].
231 Nucleolin NCL (P19338), a protein known to be involved in coronavirus processing, was also
232 predicted to bind tightly to the 5' (**Supp. Table 1**) [43].

233

234 Importantly, we found proteins related to defence response to viruses, such as ATP-dependent RNA
235 helicase DDX1 (Q92499), that are involved in negative regulation of viral genome replication.
236 Some DNA-binding proteins such as Cyclin-T1 CCNT1 (O60563), Zinc finger protein 175 ZNF175
237 (Q9Y473) and Prospero homeobox protein 1 PROX1 (Q92786) were included because they could
238 have potential RNA-binding ability (**Fig. 4E**) [44]. As for fragment 2, we found two canonical RBPs:

239 E3 ubiquitin-protein ligase TRIM32 (Q13049) and E3 ubiquitin-protein ligase TRIM21 (P19474),
240 which are listed as negative regulators of viral release from host cell, negative regulators of viral
241 transcription and positive regulators of viral entry into host cells. Among these genes, DDX1 (log
242 fold change of 0.36; p-value of 0.007 and q-value of 0.23) and TRIM21 (log fold change of 0.44; p-
243 value of 0.003 and q-value of 0.18) are the most significantly upregulated in A549 cells infected
244 with SARS-CoV-2 [40]. Finally, 10 of the 11 viral proteins detected for fragment 29 are members of
245 the Gag polyprotein family, that perform different tasks during HIV assembly, budding, maturation.
246 More than simple scaffold elements, Gag proteins are versatile elements that bind to viral and host
247 proteins as they traffic to the cell membrane (**Supp. Table 1**) [45].
248
249 Analysis of functional annotations carried out with *GeneMania* [46] revealed that proteins interacting
250 with the 5' of SARS-CoV-2 RNA are associated with regulatory pathways involving NOTCH2,
251 MYC and MAX that have been previously connected to viral infection processes (**Fig. 4E**) [47,48].
252 Interestingly, some proteins, including DDX1, CCNT1 and ZNF175 for fragment 1 and TRIM32
253 for fragment 2, have been shown to be necessary for HIV functions and replication inside the cell.
254 The roles of these proteins in retroviral replication are expected to be different in SARS-CoV-2. As
255 SARS-CoV-2 represses host gene expression through a number of unknown mechanisms [4849],
256 sequestration of elements such as DDX1 and CCNT1 could be exploited to alter biological
257 pathways in the host cell. Supporting this hypothesis, DXX1 and CCNT1 have been shown to
258 condense in large ribonucleoprotein assemblies such as stress granules [50–52] that are the primary
259 target of RNA viruses [53]. Regarding the function of these proteins in disease, DDX1 is required for
260 HIV-1 Rev as well as for avian coronavirus IBV replication and it binds to the RRE sequence of
261 HIV-1 RNAs [1–3], while CCNT1 binds to 7SK snRNA and regulates transactivation domain of the
262 viral nuclear transcriptional activator, Tat [56,57].
263
264 **Analysis of SARS-CoV-2 proteins reveals common interactions**
265
266 Recently, Gordon *et al*. reported a list of human proteins binding to Open Reading Frames (ORFs)
267 translated from SARS-CoV-2 [58]. Identified through affinity purification followed by mass
268 spectrometry quantification, 332 proteins from HEK-293T cells interact with viral ORF peptides.
269 By selecting 274 proteins binding at the 5' with Z score ≥1.5 (**Supp. Table 1**), of which 140 are
270 exclusively interacting with fragment 1 (**Fig. 4B**), we found that 8 are also reported in the list by
271 Gordon *et al*. [58], which indicates significant enrichment (representation factor of 2.5; p-value of
272 0.02; hypergeometric test with human proteome in background). The fact that our list of protein-

273 RNA binding partners contains elements identified also in the protein-protein network analysis is
274 not surprising, as ribonucleoprotein complexes evolve together [14] and their components sustain each
275 other through different types of interactions [16].
276
277 We note that out of 332 interactions, 60 are RBPs (as reported in Uniprot [39]), which represents a
278 considerable fraction (i.e., 20%), considering that there are around 1500 RBPs in the human
279 proteome (i.e., 6%) and fully justified by the fact that they involve association with viral RNA.
280 Comparing the RBPs present in Gordon *et al.* [58] and those present in our list (79 as in Uniprot), we
281 found an overlap of 6 proteins (representation factor = 26.5; p-value < 10^{-8}; hypergeometric test),
282 including: Janus kinase and microtubule-interacting protein 1 JAKMIP1 (Q96N16), A-kinase
283 anchor protein 8 AKAP8 (O43823) and A-kinase anchor protein 8-like AKAP8L (Q9ULX6), which
284 in case of HIV-1 infection is involved as a DEAD/H-box RNA helicase binding [59], signal
285 recognition particle subunit SRP72 (O76094), binding to the 7S RNA in presence of SRP68, La-
286 related protein 7, LARP7 (Q4G0J3) and La-related protein 4B LARP4B (Q92615), which are part
287 of a system for transcriptional regulation acting by means of the 7SK RNP system [60] (**Fig. 4F;**
288 **Supp. Table 2**). Interestingly, SRP72, LARP7 and LARP4B proteins assemble in stress granules
289 [61–63] that are the targeted by RNA viruses [53]. We speculate that sequestration of these elements is
290 orchestrated by a viral program aiming to recruit host genes [49]. LARP7 is also upregulated in A549
291 cells infected with SARS-CoV-2 (log fold change of 0.48; p-value of 0.006 and q-value of 0.23) [40].
292
293 Moreover, by directly analysing the RNA interaction potential of all the 332 proteins by Gordon *et*
294 *al.* [58], *cat*RAPID identified 38 putative binders at the 5' (Z score ≥ 1.5; 27 occurring exclusively in
295 the 5' and not in other regions of the RNA) [18], including Serine/threonine-protein kinase TBK1
296 (Q9UHD2), among which 10 RBPs (as reported in Uniprot) such as: Splicing elements U3 small
297 nucleolar ribonucleoprotein protein MPP10 (O00566) and Pre-mRNA-splicing factor SLU7
298 (O95391), snRNA methylphosphate capping enzyme MEPCE involved in negative regulation of
299 transcription by RNA polymerase II 7SK (Q7L2J0) [64], Nucleolar protein 10 NOL10 (Q9BSC4) and
300 protein kinase A Radixin RDX (P35241; in addition to those mentioned above; **Supp. Table 2**).
301
302 **HIV-related RBPs are significantly enriched in the 5' interactions**
303
304 In the list of 274 proteins binding to the 5' (fragment 1) with Z score ≥1.5, we found 10 hits
305 associated with HIV (**Supp. Table 3**), which represents a significant enrichment (p-value=0.0004;
306 Fisher's exact test), considering that the total number of HIV-related proteins is 35 in the whole

307 *cat*RAPID library (3340 elements). The complete list of proteins includes ATP-dependent RNA
308 helicase DDX1 (Q92499 also involved in Coronavirus replication [54,55]), ATP-dependent RNA
309 helicase DDX3X (O00571 also involved in Dengue and Zika Viruses), Tyrosine-protein kinase
310 HCK (P08631, nucleotide binding), Arf-GAP domain and FG repeat-containing protein 1 (P52594),
311 Double-stranded RNA-specific editase 1 ADARB1 (P78563), Insulin-like growth factor 2 mRNA-
312 binding protein 1 IGF2BP1 (Q9NZI8), A-kinase anchor protein 8-like AKAP8L (Q9ULX6; its
313 partner AKAP8 is also found in Gordon *et al.* [58]) Cyclin-T1 CCNT1 (O60563; DNA-binding) and
314 Forkhead box protein K2 FOXK2 (Q01167; DNA-binding; **Fig. 4B,E Supp. Table 3**).
315
316
317 Smaller enrichments were found for proteins related to Hepatitis B virus (HBV; p-value=0.01; 3
318 hits out of 7 in the whole *cat*RAPID library; Fisher's exact test), Nuclear receptor subfamily 5
319 group A member 2 NR5A2 (DNA-binding; O00482), Interferon-induced, double-stranded RNA-
320 activated protein kinase EIF2AK2 (P19525), and SRSF protein kinase 1 SRPK1 (Q96SB4) as well
321 as Influenza (p-value=0.03; 2 hits out of 4; Fisher's exact test), Synaptic functional regulator FMR1
322 (Q06787) and RNA polymerase-associated protein RTF1 homologue (Q92541; **Supp. Table 3**). By
323 contrast, no significant enrichments were found for other viruses such as for instance Ebola.
324
325 Very importantly, specific chemical compounds have been developed to interact with HIV- and
326 HVB-related proteins. The list of HIV-related targets reported in ChEMBL [65] includes ATP-
327 dependent RNA helicase DDX1 (CHEMBL2011807), ATP-dependent RNA helicase DDX3X
328 (CHEMBL2011808), Cyclin-T1 CCNT1 (CHEMBL2348842), and Tyrosine-protein kinase HCK
329 (CHEMBL2408778)[65], among other targets. In addition, HVB-related targets are Nuclear receptor
330 subfamily 5 group A member 2 NR5A2 (CHEMBL3544), Interferon-induced, double-stranded
331 RNA-activated protein kinase EIF2AK2 (CHEMBL5785) and SRSF protein kinase 1 SRPK1
332 (CHEMBL4375). We hope that this list can be the starting point for further pharmaceutical studies.
333
334 **Phase-separating proteins are enriched in the 5' interactions**
335
336 A number of proteins identified in our *cat*RAPID calculations have been previously reported to
337 coalesce in large ribonucleoprotein assemblies such as stress granules. Among these proteins, we
338 found double-stranded RNA-activated protein kinase EIF2AK2 (P19525), Nucleolin NCL
339 (P19338), ATP-dependent RNA helicase DDX1 (Q92499), Cyclin-T1 CCNT1 (O60563), signal
340 recognition particle subunit SRP72 (O76094), LARP7 (Q4G0J3) and La-related protein 4B
341 LARP4B (Q92615) as well as Polypyrimidine tract-binding protein 1 PTBP1 (P26599) and

342 Heterogeneous nuclear ribonucleoprotein Q HNRNPQ (O60506) [63]. To further investigate the
343 propensity of these proteins to phase separate in stress granules, we used the *cat*GRANULE
344 algorithm (**Materials and Methods**) [66] . We found that the 274 proteins binding to the 5' (fragment
345 1) with Z score ≥1.5 are highly prone to accumulate in stress-granules (274 proteins with the lowest
346 Z score are used in the comparison; p-value<0.0001; Kolmogorov-Smirnoff; **Fig. 4G; Supp. Table**
347 **4**).
348
349 This finding is particularly relevant because RNA viruses are known to antagonize stress granules
350 formation [53]. Indeed, the role of stress granules and processing bodies in translation suppression and
351 RNA decay have impact on virus replication [67].
352

353 **CONCLUSIONS**

354

355 Our study is motivated by the need to identify molecular mechanisms involved in Covid-19
356 spreading. Using advanced computational approaches, we investigated the structural content of
357 SARS-CoV-2 RNA and predicted human proteins that bind to it.

358

359 We employed *CROSS* [13,68] to compare the structural properties of 2800 coronaviruses and identified
360 elements conserved in SARS-CoV-2 strains. The regions containing the highest amount of structure
361 are the 5' as well as glycoproteins spike S and membrane M.

362

363 We found that the spike S protein domain encompassing amino acids 330-500 is highly conserved
364 across SARS-CoV-2 strains. This result suggests that spike S must have evolved to specifically
365 interact with its host partner ACE2 [30] and mutations increasing the binding affinity are highly
366 infrequent. As the nucleic acids encoding for this region are enriched in double-stranded content,
367 we speculate that the structure might attract host regulatory elements, thus further constraining the
368 variability. The fact that the Spike S region is highly conserved among all the analysed SARS-CoV-
369 2 strains suggests that a specific drug can be designed against it to prevent interactions within the
370 host.

371

372 By contrast, the highly variable region at amino acids 243-302 in spike S protein corresponds to the
373 binding site of sialic acids in MERS-CoV (see manuscript by E. Milanetti *et al.*) [7,10,34] and could
374 play a role in infection [33]. The fact that the binding region changes in the different strains might
375 indicate a variety of binding affinities for sialic acids, which could provide clues on the specific
376 responses in the human population. Interestingly, the sialic acid binding site is absent in SARS-CoV
377 but present in MERS-CoV, which represents an important difference between the diseases.

378

379 Both our sequence and structural analyses of spike S protein indicate high conservation among
380 coronaviruses and suggest that human engineering of SARS-CoV-2 is highly unlikely.

381

382 Using *cat*RAPID [18,19] we computed >100000 protein interactions with SARS-CoV-2 and found
383 previously reported interactions such as Polypyrimidine tract-binding protein 1 PTBP1,
384 Heterogeneous nuclear ribonucleoprotein Q HNRNPQ and Nucleolin NCL [43]. In addition, we
385 discovered that the highly structured region at the 5' has the largest number of protein partners
386 including ATP-dependent RNA helicase DDX1, which was previously reported to be essential for

387 HIV-1 and coronavirus IBV replication [54,55], and the double-stranded RNA-specific editases
388 ADAR and ADARB1, which catalyse the hydrolytic deamination of adenosine to inosine [49] . Other
389 predicted interactions are XRCC5 and XRCC6 members of the HDP-RNP complex associating
390 with ATP-dependent RNA helicase DHX9 [69] as well as and 2-5A-dependent ribonuclease RNASEL
391 and 2-5-oligoadenylate synthase 2 OAS2 that control viral RNA degradation [70,71]. Interestingly,
392 DDX1, XRCC6 and OAS2 are upregulated in human alveolar adenocarcinoma cells infected with
393 SARS-CoV-2 [40]. In agreement with our predictions, recent experimental work indicates that the
394 family of ADAR deaminases is active in bronchoalveolar lavage fluids derived from SARS-CoV-2
395 patients [42].
396
397 A significant overlap exists with the list of protein interactions reported by Gordon *et al.* [58], and
398 among the candidate partners we identified AKAP8L, involved as a DEAD/H-box RNA helicase
399 binding protein involved in HIV infection [59]. In general, proteins associated with retroviral
400 replication are expected to play different roles in SARS-CoV-2. As SARS-CoV-2 massively
401 represses host gene expression [49], we hypothesize that the virus hijacks host pathways by recruiting
402 transcriptional and post-transcriptional elements interacting with polymerase II genes and splicing
403 factors such as for instance A-kinase anchor protein 8-like AKAP8L and La-related protein 7
404 LARP7 that is upregulated in human alveolar adenocarcinoma cells infected with SARS-CoV-2 [40].
405 The link to proteins previously studied in the context of HIV and other viruses, if further confirmed
406 fro, is particularly relevant for the repurposing of existing drugs [65].
407
408 The idea that SARS-CoV-2 sequesters different elements of the transcriptional machinery is
409 particularly intriguing and is supported by the fact that a large number of proteins identified in our
410 screening are found in stress granules [63]. Indeed, stress granules protect the host innate immunity
411 and are hijacked by viruses to favour their own replication [67]. Moreover, as coronaviruses
412 transcription uses discontinuous RNA synthesis that involves high-frequency recombination [43], it is
413 possible that pieces of the viruses resulting from a mechanism called defective interfering RNAs [72]
414 could act as scaffold to attract host proteins [14,15].
415
416

Acknowledgements

The authors would like to thank Dr. Mattia Miotto, Dr Lorenzo Di Rienzo, Dr. Alexandros Armaos, Dr. Alessandro Dasti and Dr. Claudia Giambartolomei for discussions. We are particularly grateful to Prof. Annalisa Pastore for critical reading, Dr. Gilles Mirambeau for the RT vs RdRP analysis, Dr. Andrea Cerase for the discussing on stress granules and Dr. Roberto Giambruno for pointing to PTBP1 and HNRNPQ experiments.

The research leading to these results has been supported by European Research Council (RIBOMYLOME_309545 and ASTRA_855923), the H2020 projects IASIS_727658 and INFORE_825080, the Spanish Ministry of Economy and Competitiveness BFU2017-86970-P as well as the collaboration with Peter St. George-Hyslop financed by the Wellcome Trust.

Contributions. GGT and RDP conceived the study. AV carried out *cat*RAPID analysis of protein interactions, RDP calculated *CROSS* structures of coronaviruses, GGT, MM and EM performed and analysed sequence alignments, JR, EZ and EB analysed the prediction results. AV, RDP and GGT wrote the paper.

The authors do not have conflicts of interests.

437 **MATERIALS AND METHODS**

438

439 ***Structure prediction***

440

441 We predicted the secondary structure of transcripts using *CROSS* (Computational Recognition of
442 Secondary Structure [13,68]. *CROSS* was developed to perform high-throughput RNA profiling. The
443 algorithm predicts the structural profile (single- and double-stranded state) at single-nucleotide
444 resolution using sequence information only and without sequence length restrictions (scores > 0
445 indicate double stranded regions). We used the *Vienna* method [27] to further investigate the RNA
446 secondary structure of minima and maxima identified with *CROSS* [13].

447

448 ***Structural conservation***

449

450 We used *CROSS*align [13,68] an algorithm based on Dynamic Time Warping (DTW), to check and
451 evaluate the structural conservation between different viral genomes [13]. CROSS*align* was
452 previously employed to study the structural conservation of ~5000 HIV genomes. SARS-CoV-2
453 fragments (1000 nt, not overlapping) were searched inside other complete genomes using the OBE
454 (open begin and end) module, in order to search a small profile inside a larger one. The lower the
455 structural distance, the higher the structural similarities (with a minimum of 0 for almost identical
456 secondary structure profiles). The significance is assessed as in the original publication [13].

457

458 ***Sequence collection***

459

460 The FASTA sequences of the complete genomes of SARS-CoV-2 were downloaded from Virus
461 Pathogen Resource (VIPR; www.viprbrc.org), for a total of 62 strains. Regarding the overall
462 coronaviruses, the sequences were downloaded from NCBI selecting only complete genomes, for a
463 total of 2862 genomes. The reference Wuhan sequence with available annotation
464 (EPI_ISL_402119) was downloaded from Global Initiative on Sharing All Influenza Data. (GISAID
465 https://www.gisaid.org/).

466

467

468

469

470

471 ***Protein-RNA interaction prediction***

472

473 Interactions between each fragment of target sequence and the human proteome were predicted
474 using *cat*RAPID *omics* [18,19] , an algorithm that estimates the binding propensity of protein-RNA
475 pairs by combining secondary structure, hydrogen bonding and van der Waals contributions. As
476 reported in a recent analysis of about half a million of experimentally validated interactions [31], the
477 algorithm is able to separate interacting vs non-interacting pairs with an area under the ROC curve
478 of 0.78. The complete list of interactions between the 30 fragments and the human proteome is
479 available at http://crg-webservice.s3.amazonaws.com/submissions/2020-
480 03/252523/output/index.html?unlock=f6ca306af0. The output then is filtered according to the Z-
481 score column, which is the interaction propensity normalised by the mean and standard deviation
482 calculated over the reference RBP set (http://s.tartaglialab.com/static_files/shared/faqs.html#4). We
483 used three different thresholds in ascending order of stringency: Z greater or equal than 1.50, 1.75
484 and 2 respectively and for each threshold we then selected the proteins that were unique for each
485 fragment for each threshold. *omiXscore* calculations of ADAR and ADARB1 are interactions are
486 respectively at http://crg-webservice.s3.amazonaws.com/submissions/2020-
487 04/263420/output/index.html?unlock=f9375fdbf9 and http://crg-
488 webservice.s3.amazonaws.com/submissions/2020-
489 04/263140/output/index.html?unlock=bb28d715ea.

490
491

492

493 ***GO terms analysis***

494

495 *clever*GO [38], an algorithm for the analysis of Gene Ontology annotations, was used to determine
496 which fragments present enrichment in GO terms related to viral processes. Analysis of functional
497 annotations was performed in parallel with *GeneMania* [46].

498

499 ***RNA and protein alignments***

500

501 We used *Clustal W* [28] for 62 SARS-CoV-2 strains alignments and *T-Coffee* [32] for spike S proteins
502 alignments. The variability in the spike S region was measured by computing Shannon entropy on
503 translated RNA sequences. The Shannon entropy is computed as follows:

504

505 S(a) = - Sum_i P(a,i) log P(a,i)

506

507 Where *a* correspond to the amino acid at the position *i* and P(a,i) is the frequency of a certain
508 amino-acid *a* at position *i* of the sequence. Low entropy indicates poorly variability: if P(a,x) = 1 for
509 one *a* and 0 for the rest, then S(x) =0. By contrast, if the frequencies of all amino acids are equally
510 distributed, the entropy reaches its maximum possible value.

511 ***Predictions of phase separation***

512

513 *cat*GRANULE [66] was employed to identify proteins assembling into biological condensates. Scores
514 > 0 indicate that a protein is prone to phase separate. Structural disorder, nucleic acid binding
515 propensity and amino acid patterns such as arginine-glycine and phenylalanine-glycine are key
516 features combined in this computational approach [66].

517

518

519

520 **References**

521

522 1. Zhu, N. *et al.* A Novel Coronavirus from Patients with Pneumonia in China, 2019. *N. Engl. J.*
523 *Med.* **382**, 727–733 (2020).
524 2. D'Antiga, L. Coronaviruses and immunosuppressed patients. The facts during the third
525 epidemic. *Liver Transpl.* (2020) doi:10.1002/lt.25756.
526 3. Cascella, M., Rajnik, M., Cuomo, A., Dulebohn, S. C. & Di Napoli, R. Features, Evaluation and
527 Treatment Coronavirus (COVID-19). in *StatPearls* (StatPearls Publishing, 2020).
528 4. Ge, X.-Y. *et al.* Isolation and characterization of a bat SARS-like coronavirus that uses the
529 ACE2 receptor. *Nature* **503**, 535–538 (2013).
530 5. Follis, K. E., York, J. & Nunberg, J. H. Furin cleavage of the SARS coronavirus spike
531 glycoprotein enhances cell-cell fusion but does not affect virion entry. *Virology* **350**, 358–369
532 (2006).
533 6. Xiao, K. *et al.* Isolation and Characterization of 2019-nCoV-like Coronavirus from Malayan
534 Pangolins. *bioRxiv* 2020.02.17.951335 (2020) doi:10.1101/2020.02.17.951335.

535 7. Park, Y.-J. *et al.* Structures of MERS-CoV spike glycoprotein in complex with sialoside
536 attachment receptors. *Nat. Struct. Mol. Biol.* **26**, 1151–1157 (2019).
537 8. Walls, A. C. *et al.* Cryo-electron microscopy structure of a coronavirus spike glycoprotein
538 trimer. *Nature* **531**, 114–117 (2016).
539 9. Ou, X. *et al.* Characterization of spike glycoprotein of SARS-CoV-2 on virus entry and its
540 immune cross-reactivity with SARS-CoV. *Nature Communications* **11**, 1–12 (2020).
541 10. Li, W. *et al.* Identification of sialic acid-binding function for the Middle East respiratory
542 syndrome coronavirus spike glycoprotein. *Proc. Natl. Acad. Sci. U.S.A.* **114**, E8508–E8517
543 (2017).
544 11. Yang, D. & Leibowitz, J. L. The Structure and Functions of Coronavirus Genomic 3' and 5'
545 Ends. *Virus Res* **206**, 120–133 (2015).
546 12. Delli Ponti, R., Marti, S., Armaos, A. & Tartaglia, G. G. A high-throughput approach to profile
547 RNA structure. *Nucleic Acids Res* **45**, e35–e35 (2017).
548 13. Delli Ponti, R., Armaos, A., Marti, S. & Gian Gaetano Tartaglia. A Method for RNA Structure
549 Prediction Shows Evidence for Structure in lncRNAs. *Front Mol Biosci* **5**, 111 (2018).
550 14. Sanchez de Groot, N. *et al.* RNA structure drives interaction with proteins. *Nat Commun* **10**,
551 3246 (2019).
552 15. Cid-Samper, F. *et al.* An Integrative Study of Protein-RNA Condensates Identifies Scaffolding
553 RNAs and Reveals Players in Fragile X-Associated Tremor/Ataxia Syndrome. *Cell Rep* **25**,
554 3422-3434.e7 (2018).
555 16. Cerase, A. *et al.* Phase separation drives X-chromosome inactivation: a hypothesis. *Nature*
556 *Structural & Molecular Biology* **26**, 331 (2019).
557 17. Moreno, J. L., Zúñiga, S., Enjuanes, L. & Sola, I. Identification of a Coronavirus Transcription
558 Enhancer. *Journal of Virology* **82**, 3882–3893 (2008).
559 18. Agostini, F. *et al.* catRAPID omics: a web server for large-scale prediction of protein-RNA
560 interactions. *Bioinformatics* **29**, 2928–2930 (2013).

561 19. Cirillo, D. *et al.* Quantitative predictions of protein interactions with long noncoding RNAs. *Nat*
562 *Meth* **14**, 5–6 (2017).
563 20. Bellucci, M., Agostini, F., Masin, M. & Tartaglia, G. G. Predicting protein associations with
564 long noncoding RNAs. *Nat. Methods* **8**, 444–445 (2011).
565 21. Lang, B., Armaos, A. & Tartaglia, G. G. RNAct: Protein–RNA interaction predictions for
566 model organisms with supporting experimental data. *Nucleic Acids Res*
567 doi:10.1093/nar/gky967.
568 22. Kliger, Y. & Levanon, E. Y. Cloaked similarity between HIV-1 and SARS-CoV suggests an
569 anti-SARS strategy. *BMC Microbiol* **3**, 20 (2003).
570 23. Hallenberger, S. *et al.* Inhibition of furin-mediated cleavage activation of HIV-1 glycoprotein
571 gp160. *Nature* **360**, 358–361 (1992).
572 24. Glowacka, I. *et al.* Differential downregulation of ACE2 by the spike proteins of severe acute
573 respiratory syndrome coronavirus and human coronavirus NL63. *J. Virol.* **84**, 1198–1205
574 (2010).
575 25. Gultyaev, A. P., Richard, M., Spronken, M. I., Olsthoorn, R. C. L. & Fouchier, R. A. M.
576 Conserved structural RNA domains in regions coding for cleavage site motifs in hemagglutinin
577 genes of influenza viruses. *Virus Evol* **5**, (2019).
578 26. Wu, A. *et al.* Genome Composition and Divergence of the Novel Coronavirus (2019-nCoV)
579 Originating in China. *Cell Host Microbe* **27**, 325–328 (2020).
580 27. Lorenz, R. *et al.* ViennaRNA Package 2.0. *Algorithms for Molecular Biology* **6**, 26 (2011).
581 28. Madeira, F. *et al.* The EMBL-EBI search and sequence analysis tools APIs in 2019. *Nucleic*
582 *Acids Res* **47**, W636–W641 (2019).
583 29. Hrdlickova, R., Toloue, M. & Tian, B. RNA-Seq methods for transcriptome analysis. *Wiley*
584 *Interdiscip Rev RNA* **8**, (2017).
585 30. Andersen, K. G., Rambaut, A., Lipkin, W. I., Holmes, E. C. & Garry, R. F. The proximal origin
586 of SARS-CoV-2. *Nature Medicine* 1–3 (2020) doi:10.1038/s41591-020-0820-9.

587 31. Zhou, P. *et al.* A pneumonia outbreak associated with a new coronavirus of probable bat origin.
588 *Nature* **579**, 270–273 (2020).
589 32. Di Tommaso, P. *et al.* T-Coffee: a web server for the multiple sequence alignment of protein
590 and RNA sequences using structural information and homology extension. *Nucleic Acids Res*
591 **39**, W13–W17 (2011).
592 33. Qing, E., Hantak, M., Perlman, S. & Gallagher, T. Distinct Roles for Sialoside and Protein
593 Receptors in Coronavirus Infection. *mBio* **11**, (2020).
594 34. Milanetti, E. *et al.* In-Silico evidence for two receptors based strategy of SARS-CoV-2.
595 *arXiv:2003.11107 [physics, q-bio]* (2020).
596 35. Galán, C. *et al.* Host cell proteins interacting with the 3' end of TGEV coronavirus genome
597 influence virus replication. *Virology* **391**, 304–314 (2009).
598 36. Lu, K., Heng, X. & Summers, M. F. Structural determinants and mechanism of HIV-1 genome
599 packaging. *J. Mol. Biol.* **410**, 609–633 (2011).
600 37. Fehr, A. R. & Perlman, S. Coronaviruses: An Overview of Their Replication and Pathogenesis.
601 *Methods Mol Biol* **1282**, 1–23 (2015).
602 38. Klus, P., Ponti, R. D., Livi, C. M. & Tartaglia, G. G. Protein aggregation, structural disorder
603 and RNA-binding ability: a new approach for physico-chemical and gene ontology
604 classification of multiple datasets. *BMC Genomics* **16**, 1071 (2015).
605 39. UniProt: a worldwide hub of protein knowledge. *Nucleic Acids Res* **47**, D506–D515 (2019).
606 40. Blanco-Melo, D. *et al.* SARS-CoV-2 launches a unique transcriptional signature from in vitro,
607 ex vivo, and in vivo systems. *bioRxiv* 2020.03.24.004655 (2020)
608 doi:10.1101/2020.03.24.004655.
609 41. Armaos, A., Cirillo, D. & Gaetano Tartaglia, G. omiXcore: a web server for prediction of
610 protein interactions with large RNA. *Bioinformatics* (2017) doi:10.1093/bioinformatics/btx361.

611 42. Giorgio, S. D., Martignano, F., Torcia, M. G., Mattiuz, G. & Conticello, S. G. Evidence for
612 host-dependent RNA editing in the transcriptome of SARS-CoV-2. *bioRxiv* 2020.03.02.973255
613 (2020) doi:10.1101/2020.03.02.973255.
614 43. Sola, I., Mateos-Gomez, P. A., Almazan, F., Zuñiga, S. & Enjuanes, L. RNA-RNA and RNA-
615 protein interactions in coronavirus replication and transcription. *RNA Biol* **8**, 237–248 (2011).
616 44. Castello, A. *et al.* Insights into RNA biology from an atlas of mammalian mRNA-binding
617 proteins. *Cell* **149**, 1393–1406 (2012).
618 45. Bell, N. M. & Lever, A. M. L. HIV Gag polyprotein: processing and early viral particle
619 assembly. *Trends in Microbiology* **21**, 136–144 (2013).
620 46. Warde-Farley, D. *et al.* The GeneMANIA prediction server: biological network integration for
621 gene prioritization and predicting gene function. *Nucleic Acids Res* **38**, W214–W220 (2010).
622 47. Hayward, S. D. Viral interactions with the Notch pathway. *Semin. Cancer Biol.* **14**, 387–396
623 (2004).
624 48. Dudley, J. P., Mertz, J. A., Rajan, L., Lozano, M. & Broussard, D. R. What retroviruses teach
625 us about the involvement of c- Myc in leukemias and lymphomas. *Leukemia* **16**, 1086–1098
626 (2002).
627 49. Kim, D. *et al.* The architecture of SARS-CoV-2 transcriptome. *bioRxiv (now Cell in press)*
628 2020.03.12.988865 (2020) doi:10.1101/2020.03.12.988865.
629 50. Ning, W. *et al.* DrLLPS: a data resource of liquid–liquid phase separation in eukaryotes.
630 *Nucleic Acids Res* **48**, D288–D295 (2020).
631 51. Shin, Y. *et al.* Liquid Nuclear Condensates Mechanically Sense and Restructure the Genome.
632 *Cell* **175**, 1481-1491.e13 (2018).
633 52. Su, X. *et al.* Phase separation of signaling molecules promotes T cell receptor signal
634 transduction. *Science* **352**, 595–599 (2016).
635 53. White, J. P. & Lloyd, R. E. Regulation of stress granules in virus systems. *Trends Microbiol* **20**,
636 175–183 (2012).

637 54. Fang, J. *et al.* A DEAD box protein facilitates HIV-1 replication as a cellular co-factor of Rev.
638 *Virology* **330**, 471–480 (2004).
639 55. Xu, L. *et al.* The cellular RNA helicase DDX1 interacts with coronavirus nonstructural protein
640 14 and enhances viral replication. *J. Virol.* **84**, 8571–8583 (2010).
641 56. Ivanov, D. *et al.* Cyclin T1 domains involved in complex formation with Tat and TAR RNA are
642 critical for tat-activation. *J. Mol. Biol.* **288**, 41–56 (1999).
643 57. Kwak, Y. T., Ivanov, D., Guo, J., Nee, E. & Gaynor, R. B. Role of the human and murine cyclin
644 T proteins in regulating HIV-1 tat-activation. *J. Mol. Biol.* **288**, 57–69 (1999).
645 58. Gordon, D. E. *et al.* A SARS-CoV-2-Human Protein-Protein Interaction Map Reveals Drug
646 Targets and Potential Drug-Repurposing. *bioRxiv* 2020.03.22.002386 (2020)
647 doi:10.1101/2020.03.22.002386.
648 59. Xing, L., Zhao, X., Guo, F. & Kleiman, L. The role of A-kinase anchoring protein 95-like
649 protein in annealing of tRNALys3 to HIV-1 RNA. *Retrovirology* **11**, 58 (2014).
650 60. Markert, A. *et al.* The La-related protein LARP7 is a component of the 7SK ribonucleoprotein
651 and affects transcription of cellular and viral polymerase II genes. *EMBO Rep.* **9**, 569–575
652 (2008).
653 61. Schäffler, K. *et al.* A stimulatory role for the La-related protein 4B in translation. *RNA* **16**,
654 1488–1499 (2010).
655 62. Küspert, M. *et al.* LARP4B is an AU-rich sequence associated factor that promotes mRNA
656 accumulation and translation. *RNA* **21**, 1294–1305 (2015).
657 63. Markmiller, S. *et al.* Context-Dependent and Disease-Specific Diversity in Protein Interactions
658 within Stress Granules. *Cell* **172**, 590-604.e13 (2018).
659 64. C, J. *et al.* Systematic Analysis of the Protein Interaction Network for the Human Transcription
660 Machinery Reveals the Identity of the 7SK Capping Enzyme. *Molecular cell* vol. 27
661 https://pubmed.ncbi.nlm.nih.gov/17643375/ (2007).

662 65. Mendez, D. *et al.* ChEMBL: towards direct deposition of bioassay data. *Nucleic Acids Res* **47**,
663 D930–D940 (2019).
664 66. Bolognesi, B. *et al.* A Concentration-Dependent Liquid Phase Separation Can Cause Toxicity
665 upon Increased Protein Expression. *Cell Reports* **16**, 222–231 (2016).
666 67. Zhang, Q., Sharma, N. R., Zheng, Z.-M. & Chen, M. Viral Regulation of RNA Granules in
667 Infected Cells. *Virol. Sin.* **34**, 175–191 (2019).
668 68. Delli Ponti, R., Marti, S., Armaos, A. & Tartaglia, G. G. A high-throughput approach to profile
669 RNA structure. *Nucleic Acids Research* **45**, e35–e35 (2017).
670 69. Zhang, S., Schlott, B., Görlach, M. & Grosse, F. DNA-dependent protein kinase (DNA-PK)
671 phosphorylates nuclear DNA helicase II/RNA helicase A and hnRNP proteins in an RNA-
672 dependent manner. *Nucleic Acids Res* **32**, 1–10 (2004).
673 70. Sarkar, S. N., Ghosh, A., Wang, H. W., Sung, S. S. & Sen, G. C. The nature of the catalytic
674 domain of 2'-5'-oligoadenylate synthetases. *J. Biol. Chem.* **274**, 25535–25542 (1999).
675 71. Sarkar, S. N., Bandyopadhyay, S., Ghosh, A. & Sen, G. C. Enzymatic characteristics of
676 recombinant medium isozyme of 2'-5' oligoadenylate synthetase. *J. Biol. Chem.* **274**, 1848–
677 1855 (1999).
678 72. Pathak, K. B. & Nagy, P. D. Defective Interfering RNAs: Foes of Viruses and Friends of
679 Virologists. *Viruses* **1**, 895–919 (2009).
680
681
682

683 **FIGURES LEGENDS**

684

685 ***Fig. 1.*** *Using the CROSS approach* [13,68]*, we studied the structural content of SARS-CoV-2. We*
686 *found the highest density of double-stranded regions in the 5' (nucleotides 1-253), membrane M*
687 *protein (nucleotides 26523-27191), and the spike S protein (nucleotides 23000-24000). Strong*
688 *match is observed between CROSS and Vienna analyses (centroid structures shown), indicating*
689 *that regions with the highest structural content have the lowest free energies.*

690

691 ***Fig. 2.*** *We employed the CROSSalign approach* [13,68] *to compare the Wuhan strain MN908947 with*
692 *other coronaviruses (1387 strains, including SARS-CoV and MERS-CoV) indicates that the most*
693 *conserved region falls inside the spike S genomic locus. The inset shows thermodynamic structural*
694 *variability (positional entropy) within regions encompassing nucleotides 23000-24000 along with*
695 *the centroid structure and free energy.*

696

697 ***Fig. 3.*** *Sequence and structural comparison of human SARS-CoV-2 strains. (**A**) Strong sequence*
698 *conservation (Clustal W multiple sequence alignments* [38]*) is observed in coding regions, including*
699 *the region between nucleotides 23000 and 24000 of spike S protein. High structural variability (red*
700 *bars on top) is observed for both the UTRs and for nucleotides between 21000 and 22000 as well as*
701 *24000 and 25000, associated with the S region. The rest of the regions are significantly conserved*
702 *at a structural level. (**B**) The sequence variability (Shannon entropy computed on T-Coffee multiple*
703 *sequence alignments* [32]*) in the spike S protein indicate conservation between amino-acids 460 and*
704 *520 (blue box) binding to the host receptor angiotensin-converting enzyme 2 ACE2. The region*
705 *encompassing amino-acids 243 and 302 is highly variable and is implicated in sialic acids in*
706 *MERS-CoV (red box). The S1 and S2 domains of Spike S protein are displayed.*

707

708 ***Fig. 4.*** *Characterization of protein interactions with SARS-CoV-2 RNA. (**A**) In agreement with*
709 *studies on coronaviruses* [35]*, PTBP1 shows the highest interaction propensity at the 5' and*
710 *HNRNPQ at 3' (indicated by red bars). (**B**) Number of RBP interactions for different SARS-CoV-2*
711 *regions (colours indicate catRAPID* [18,19] *confidence levels: Z=1.5 or low Z=1.75 or medium and*
712 *Z=2.0 or high; regions with scores lower than Z=1.5 are omitted); (**C**) Enrichment of viral*
713 *processes in the 5' of SARS-CoV-2 (precision = term precision calculated from the GO graph*
714 *structure lvl = depth of the term; go_term = GO term identifier, with link to term description at*
715 *AmiGO website; description = label for the term; e/d = enrichment / depletion compared to the*
716 *population; %_set = coverage on the provided set; %_pop = coverage of the same term on the*

population; p_bonf = p-value of the enrichment. To correct for multiple testing bias, use Bonferroni correction) [38]*; (**D**) Viral processes are the third largest cluster identified in our analysis; (**E**) Protein interactions with the 5' of SARS-CoV-2 RNA (inner circle) and associations with other human genes retrieved from literature (green: genetic associations; pink: physical associations); (**F**) Number of RBP interactions identified by Gordon et al.* [58] *for different SARS-CoV-2 regions (see panel A for reference). (**G**) Proteins binding to the 5' with Z score ≥ 1.5 show high propensity to accumulate in stress-granules (same number of proteins with Z score* < -1.5 *are used in the comparison; *** p-value<0.0001; Kolmogorov-Smirnoff).*

725 **SUPPLEMENTARY MATERIAL**

726

727

728 ***Supp. Figure 1.*** *We employed CROSSalign* [13,68] *was to compare the Wuhan strain MN908947 with*
729 *other coronaviruses (2800 strains, including SARS-CoV, MERS-CoV and coronaviruses having as*
730 *host other species, such as bats). The result highlights that the most conserved region falls inside*
731 *the spike S genomic locus.*

732

733 ***Supp. Table 1.*** *1) catRAPID* [18,19] *score for interactions with fragment 1; 2) GO* [38] *and Uniprot*
734 *annotations of viral proteins interacting with fragment 1 and ; 3) catRAPID score for interactions*
735 *with fragment 2; 4) GO annotations of viral proteins interacting with fragment 2; 5) catRAPID*
736 *score for interactions with fragment 29; 6) GO annotations of viral proteins interacting with*
737 *fragment 29;*

738

739 ***Supp. Table 2.*** *RBP interactions from Gordon et al.* [58] *classified according to catRAPID scores.*
740 *GO* [38] *and Uniprot* [39] *annotations are reported.*

741

742 ***Supp. Table 3****. RBPs significantly enriched in the 5' with GO* [38] *and Uniprot* [39] *annotations for*
743 *HIV, HBV and Influenza.*

744

745 ***Supp. Table 4****. Stress granule propensity computed with catGRANULE* [66] *for proteins with*
746 *interactions score* $Z \geq 1.5$ *(top-ranked) and* $Z<-1.5$ *(bottom-ranked). The two groups of proteins*
747 *have the same number of elements.*

748

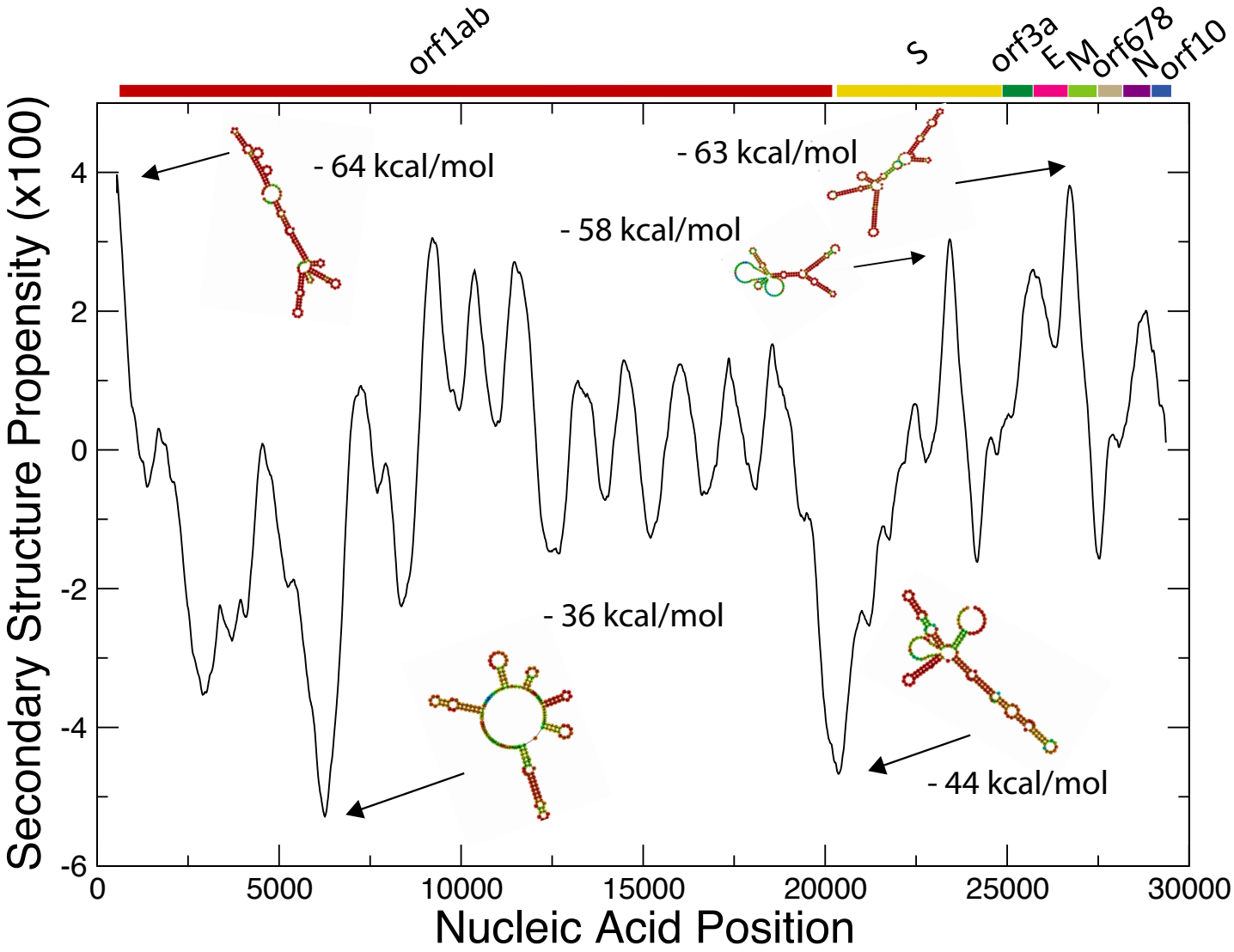
orf1ab
S
orf3a
E
M
orf678
N
orf10
- 64 kcal/mol
- 63 kcal/mol
- 58 kcal/mol
- 36 kcal/mol
- 44 kcal/mol
Secondary Structure Propensity (x100)
4
2
0
-2
-4
-6
0
5000
10000
15000
20000
25000
30000
Nucleic Acid Position

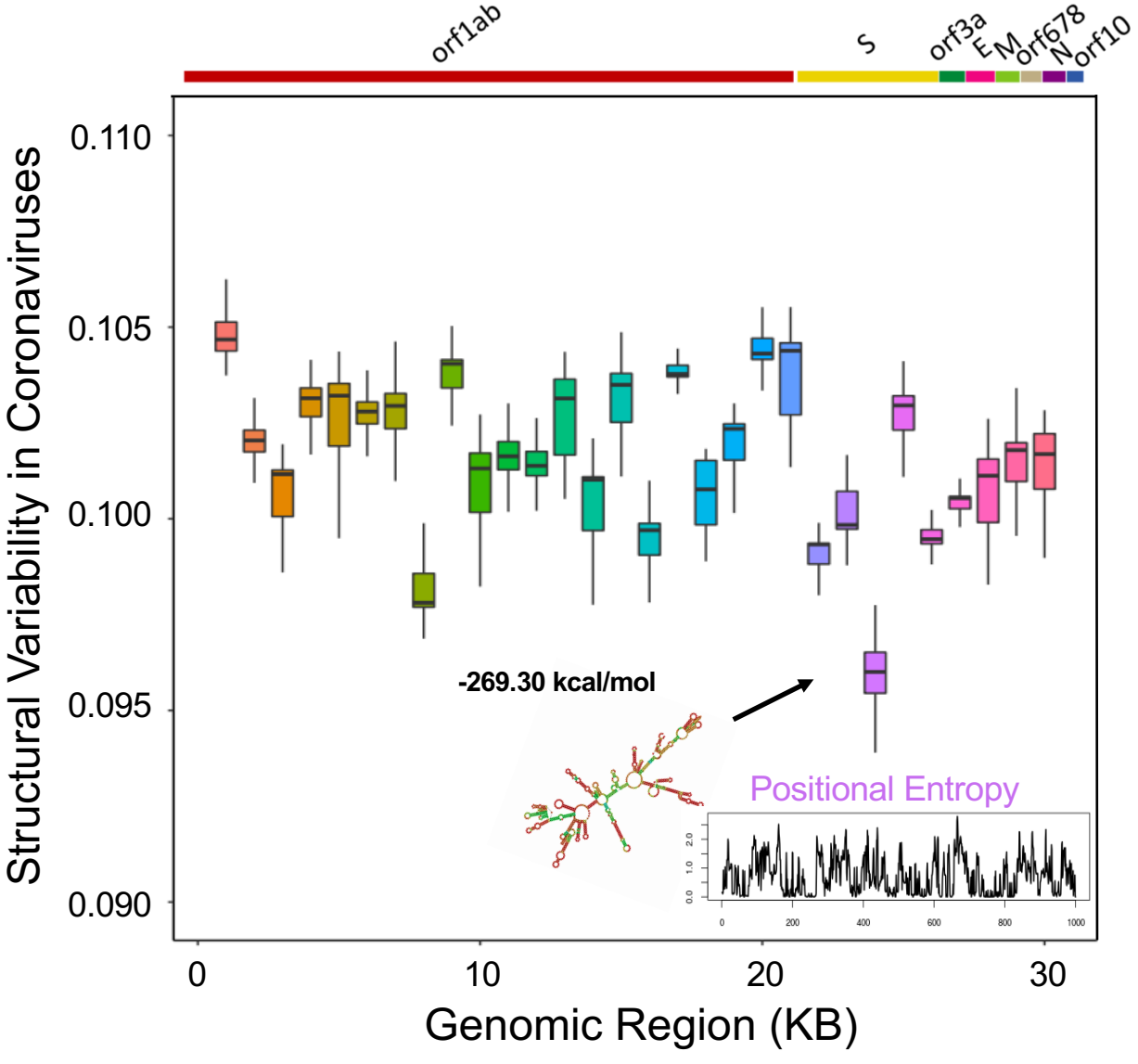
orf1ab
S
orf3a
E
M
orf678
N
orf10
Structural Variability in Coronaviruses
0.110
0.105
0.100
0.095
0.090
-269.30 kcal/mol
Positional Entropy
0
200
400
600
800
1000
0
10
20
30
Genomic Region (KB)

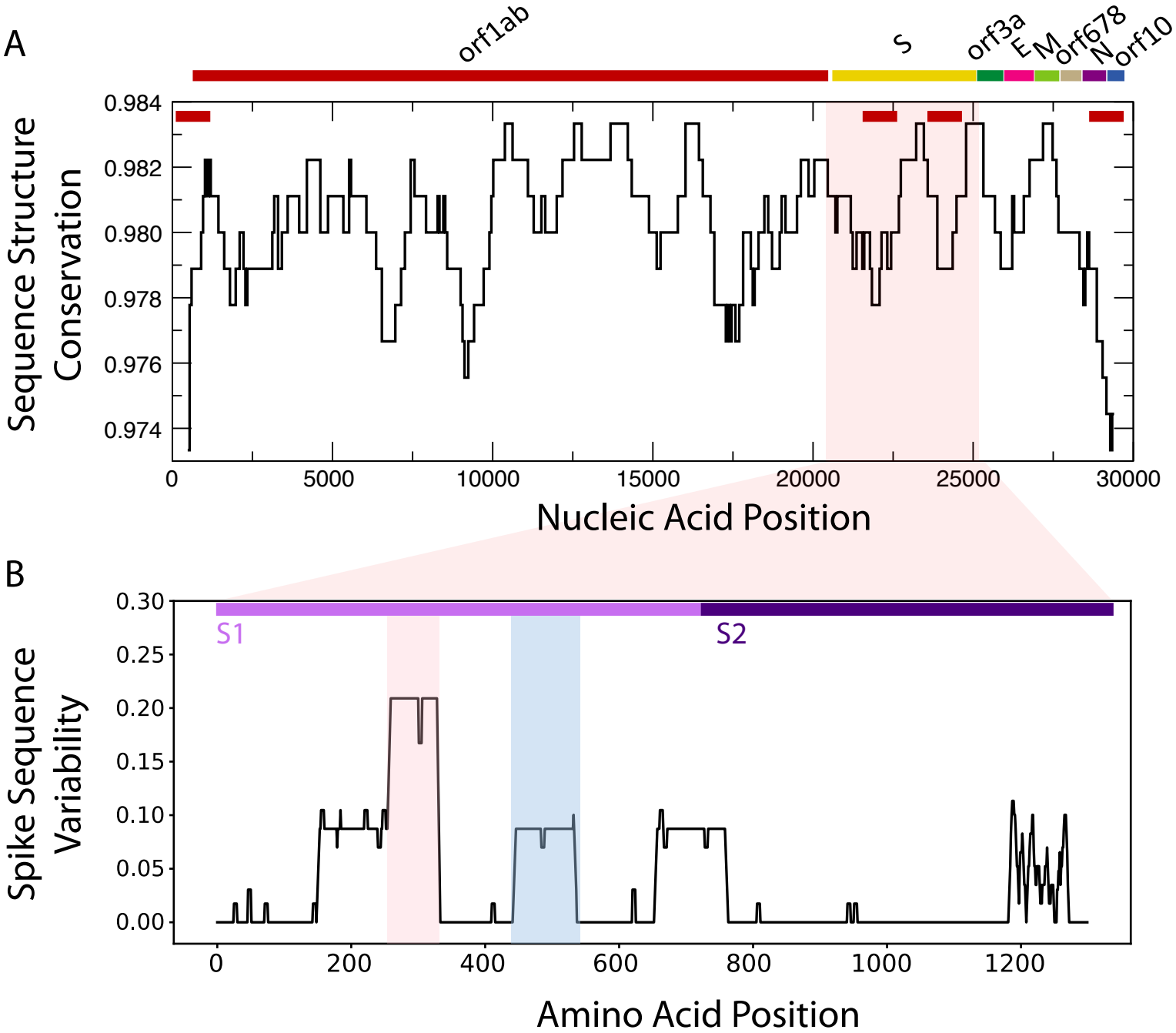
A
orf1ab
S
orf3a
E
M
orf678
N
orf10
Sequence Structure Conservation
0.984
0.982
0.980
0.978
0.976
0.974
0
5000
10000
15000
20000
25000
30000
Nucleic Acid Position
B
S1
S2
Spike Sequence Variability
0.30
0.25
0.20
0.15
0.10
0.05
0.00
0
200
400
600
800
1000
1200
Amino Acid Position

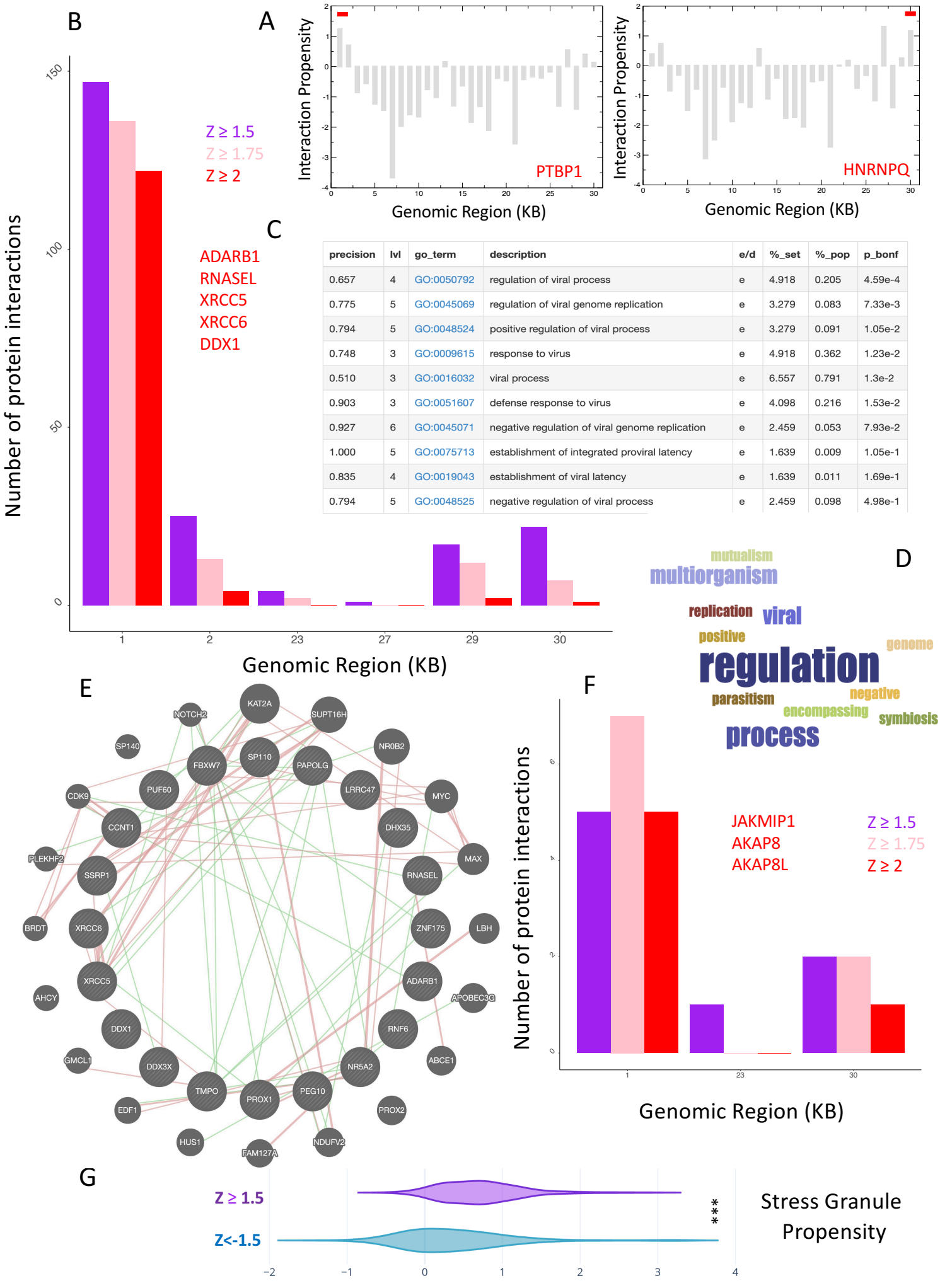

precision	lvl	go_term	description	e/d	%_set	%_pop	p_bonf
0.657	4	GO:0050792	regulation of viral process	e	4.918	0.205	4.59e-4
0.775	5	GO:0045069	regulation of viral genome replication	e	3.279	0.083	7.33e-3
0.794	5	GO:0048524	positive regulation of viral process	e	3.279	0.091	1.05e-2
0.748	3	GO:0009615	response to virus	e	4.918	0.362	1.23e-2
0.510	3	GO:0016032	viral process	e	6.557	0.791	1.3e-2
0.903	3	GO:0051607	defense response to virus	e	4.098	0.216	1.53e-2
0.927	6	GO:0045071	negative regulation of viral genome replication	e	2.459	0.053	7.93e-2
1.000	5	GO:0075713	establishment of integrated proviral latency	e	1.639	0.009	1.05e-1
0.835	4	GO:0019043	establishment of viral latency	e	1.639	0.011	1.69e-1
0.794	5	GO:0048525	negative regulation of viral process	e	2.459	0.098	4.98e-1